Available online at www.sciencedirect.com
ScienceDirect
Catalysis Today 126 (2007) 420–429
CATALYSIS TODAY
www.elsevier.com/locate/cattod

Nanosized perovskite-type oxides $La_{1-x}Sr_xMO_{3-\delta}$ (M = Co, Mn; $x = 0$, 0.4) for the catalytic removal of ethylacetate

Jianrong Niu, Jiguang Deng, Wei Liu, Lei Zhang, Guozhi Wang, Hongxing Dai *, Hong He, Xuehong Zi

Laboratory of Catalysis Chemistry and Nanoscience, Department of Chemistry and Chemical Engineering, College of Environmental and Energy Engineering, Beijing University of Technology, Beijing 100022, PR China

Available online 12 July 2007

Abstract

Nanometer perovskite-type oxides $La_{1-x}Sr_xMO_{3-\delta}$ (M = Co, Mn; $x = 0$, 0.4) have been prepared using the citric acid complexing-hydrothermal-coupled method and characterized by means of techniques, such as X-ray diffraction (XRD), BET, high-resolution scanning electron microscopy (HRSEM), X-ray photoelectron spectroscopy (XPS), temperature-programmed desorption (TPD), and temperature-programmed reduction (TPR). The catalytic performance of these nanoperovskites in the combustion of ethylacetate (EA) has also been evaluated. The XRD results indicate that all the samples possessed single-phase rhombohedral crystal structures. The surface areas of these nanomaterials ranged from 20 to 33 $m^2\ g^{-1}$, the achievement of such high surface areas are due to the uniform morphology with the typical particle size of 40–80 nm (as can be clearly seen in their HRSEM images) that were derived with the citric acid complexing-hydrothermally coupled strategy. The XPS results demonstrate the presence of Mn^{4+} and Mn^{3+} in $La_{1-x}Sr_xMnO_{3-\delta}$ and Co^{3+} and Co^{2+} in $La_{1-x}Sr_xCoO_{3-\delta}$, Sr substitution induced the rises in Mn^{4+} and Co^{3+} concentrations; adsorbed oxygen species (O^-, O_2^-, or O_2^{2-}) were detected on the catalyst surfaces. The O_2-TPD profiles indicate that Sr doping increased desorption of the adsorbed oxygen and lattice oxygen species at low temperatures. The H_2-TPR results reveal that the nanoperovskite catalysts could be reduced at much lower temperatures (<240 °C) after Sr doping. It is observed that under the conditions of EA concentration = 1000 ppm, EA/oxygen molar ratio = 1/400, and space velocity = 20,000 h^{-1}, the catalytic activity (as reflected by the temperature ($T_{100\%}$) for EA complete conversion) increased in the order of $LaCoO_{2.91}$ ($T_{100\%}$ = 230 °C) ≈ $LaMnO_{3.12}$ ($T_{100\%}$ = 235 °C) < $La_{0.6}Sr_{0.4}MnO_{3.02}$ ($T_{100\%}$ = 190 °C) < $La_{0.6}Sr_{0.4}CoO_{2.78}$ ($T_{100\%}$ = 175 °C); furthermore, there were no formation of partially oxidized by-products over these catalysts. Based on the above results, we conclude that the excellent catalytic performance is associated with the high surface areas, good redox properties (derived from higher Mn^{4+}/Mn^{3+} and Co^{3+}/Co^{2+} ratios), and rich lattice defects of the nanostructured $La_{1-x}Sr_xMO_{3-\delta}$ materials.

Keywords: Perovskite-type oxide catalysts; Nonstoichiometry; Volatile organic compounds; Ethylacetate; Catalytic oxidation; VOC combustion

1. Introduction

Volatile organic compounds (VOCs) emitted from industrial processes and transportation activities have been considered as great contributors to the atmospheric pollution [1,2]. Heterogeneous catalytic combustion of VOCs in air on solid catalysts is believed to be one of the most effective pathways [3–6], and its efficiency is determined by the catalytic activity, selectivity, and stability of the catalyst employed. Among the catalysts investigated so far, perovskite-type oxides (ABO_3) are promising catalytic materials for the total oxidation of hydrocarbons and oxygenates [7–9] due to their much lower cost as compared to noble metals. It has been proven that among the perovskites the ones with the La partially substituted by Sr in the A-site and Mn or Co in the B-site, i.e., $La_{1-x}Sr_xMO_{3-\delta}$ (M = Co, Mn; x = 0–0.4), show the best catalytic performance [10–14]. The redox properties of the M ions, the nature and concentration of oxygen adspecies, and the existence of lattice defects are generally believed to be responsible for the good catalytic activity of these perovskite-type oxides [15,16].

Ethylacetate (EA) is a good model compound of VOCs. Over γ-Al_2O_3-supported group VIII metal (Ni, Co, Ru, Pd, Pt)

* Corresponding author. Tel.: +86 10 6739 6588; fax: +86 10 6739 1983.
E-mail address: hxdai@bjut.edu.cn (H. Dai).

0920-5861/$ – see front matter © 2007 Elsevier B.V. All rights reserved.
doi:10.1016/j.cattod.2007.06.027

catalysts for the total oxidation of a VOC mixture containing benzene, *n*-butanol, and EA [17], EA was proved to exhibit the lowest oxidation reactivity, two orders of magnitude lower than benzene and *n*-butanol oxidation. Over the Pt/Al_2O_3 catalysts [18], EA was partially oxidized to acetic acid at low EA conversion, whereas under the conditions of EA conversion >90%, space velocity = 30,000 h^{-1}, and above 300 °C, the selectivity of CO_2 was only 95%, indicating that some partially oxidized products were also formed. In other words, EA is relatively difficult to be fully oxidized into CO_2 over such catalysts. In recent years, several researchers investigated the combustion of some VOCs over the Co- or Mn-based perovskite oxide catalysts [9,12,19,20], and observed that the enhancement of catalytic activity was associated with the high surface area and high defect density. The phenomenon that $LaMnO_{3-\delta}$ outperforms $LaCoO_{3-\delta}$ under similar reaction conditions was explained to be due to higher reactivity to the adsorption of VOCs over the former catalyst than that over the latter one [19]; the partial substitution of La by Sr (i.e., $A = La_{0.8}Sr_{0.2}$) resulted in the improvement of catalytic performance of $ABO_{3-\delta}$ (B = Co, Mn) [12]; over $La_{0.8}Sr_{0.2}MnO_{3-\delta}$ ($\delta < 0$), partially oxidized compounds, such as acetaldehyde (maximum yield ≈ 15%) and ethanol (maximum yield ≈ 3%) were detected at 159 °C and 20,000 h^{-1} (where EA conversion reached 99%) [20].

The major drawback of traditional perovskite-type oxides is low surface areas that limit their catalytic performance. In fact, the preparation of perovskite-type oxides with sufficiently high surface areas is a big challenge since it involves a solid-state reaction of the precursor oxides to form the characteristic $ABO_{3-\delta}$ structure. This requires significant exposure time at high temperatures, leading to a low-surface-area catalyst. In order to prevent such a limitation, a number of alternative preparation strategies have been tried, with the aim of reducing the calcination temperature necessary for perovskite phase formation. It seems that the citric acid complexing method is very effective to increase the surface area of the synthesized perovskite. The preservation of surface area is critical because the reaction rate over bulk perovskites has often been observed to be directly proportional to the BET surface area [21], especially in the case of complete oxidation of hydrocarbons and oxygenates. In the past years, we have investigated perovskite-type oxide and halo-oxide catalysts for the oxidation of carbon monoxide [22–24], the purification of automotive exhaust [23], and the oxidative dehydrogenation of ethane [25–27] as well as the decomposition of NO [24], and found that most of them performed well. Recently, we have made an attempt to prepare several series of nanometer perovskite-type oxides with high surface areas using a strategy of citric acid complexing method coupled with a hydrothermal process, and observed that these nanomaterials showed excellent catalytic activity in the total oxidation of VOCs. In this paper, we report the making, characterization, and catalytic properties of high-surface-area $La_{1-x}Sr_xMO_{3-\delta}$ (M = Co, Mn; $x = 0$, 0.4) nanoparticles for the oxidative removal of EA.

2. Experimental

2.1. Catalyst preparation

$La_{1-x}Sr_xMO_{3-\delta}$ (M = Co, Mn; $x = 0$, 0.4) catalysts were prepared using the strategy of citric acid complexing coupled with hydrothermal method. Stoichiometric amounts of nitrates of lanthanum, strontium, cobalt or manganese and equal amount of citric acid (metal/citric acid molar ratio = 1/1) were dissolved in deionized water so that the metal ions can be uniformly complexed together. A certain amount of ammonia (28 wt.%) solution was added dropwise to the above mixed solution. Part of ammonia added neutralized the unreacted citric acid. When the pH value of the solution reached near 9.2, a sol was obtained. Then this sol was transferred to a 50 ml autoclave with the packed volume = 40 ml and the autoclave was placed into an oven for hydrothermal treatment at 150 °C for 20 h. The obtained precursors were in turn filtered, washed with deionized water, filtered again, and dried at 120 °C for 5 h. The dried powders were well ground and calcined in air in a muffle furnace with the temperature ramp of 1 °C min^{-1}, and kept at 400 °C for 2 h and 650 °C (700 °C for $LaMnO_{3-\delta}$ due to less crystalline at 650 °C) for 2 h, respectively. We also calcined the Sr-doped cobalt and manganite catalysts at 900 °C for 4 h for the purpose of comparing their catalytic performance with those derived at 650 °C calcination. Finally, the as-received powders were ground, tabletted, crushed, and sieved to a size range of 40–60 mesh.

2.2. Catalyst characterization

The crystal structures of the catalysts were determined by an X-ray diffractometer (XRD, 8D Advance, Rigaku) operating at 40 kV and 200 mA using Cu Kα radiation and Ni filter. The patterns recorded were referred to the powder diffraction files-1998 ICDD PDF Database for phase identification. The specific surface areas of the catalysts were measured using N_2 adsorption at −196 °C on an ASAP 2020 apparatus. X-ray photoelectron spectroscopy (XPS, VG CLAM 4 MCD analyzer) was used to determine the O 1s, Co 2p, and Mn 2p binding energies of surface oxygen, cobalt, and manganese species with Mg Kα ($h\nu = 1253.6$ eV) as the excitation source. The instrumental resolution is 0.5 eV. Before XPS measurements, the samples were calcined in O_2 (flow rate, 20 ml min^{-1}) at 600 °C for 1 h and then cooled to room temperature. After the above treatment, the samples were mounted and transferred to the spectrometer in a transparent GLOVE BAG (Instruments for Research and Industry, USA) filled with helium to avoid exposure to the air. Finally, the samples were outgassed in the primary vacuum chamber (10^{-5} Torr) for 0.5 h and then introduced into the ultrahigh vacuum chamber (3×10^{-9} Torr) for recording. The C 1s line at 284.6 eV was taken as a reference for binding energy calibration. The high-resolution scanning electron microscopy (HRSEM) images of the samples were recorded using the JEOL JSM 6500F equipment operated at a 30.0 kV accelerating voltage.

For the O_2-TPD (temperature-programmed desorption) studies, the sample (0.1–0.2 g) was placed in the middle of a quartz microreactor of 8 mm i.d. The outlet gases were analyzed on-line by mass spectrometry (HIDEN HPR20). The heating rate was 10 °C min^{-1} and the temperature range was 30–900 °C. Before an O_2-TPD experiment, the sample was calcined in O_2 (flow rate, 20 ml min^{-1}) for 1 h, followed by cooling in oxygen to room temperature and helium purging (first 80 ml min^{-1} for 2 h and then 20 ml min^{-1} for 2 h). The helium-purging step is aimed to remove all the gas-phase oxygen in the system. The amount of O_2 desorbed from the catalyst was quantified by calibrating the peak area against that of a standard pulse (50.0 μl). Temperature-programmed reduction (TPR) was conducted by using a 5% H_2–95% Ar (v/v) mixture. The flow rate of the carrier gas was 50 ml min^{-1} and a thermal conductivity detector was adopted. The amount of the sample used was 0.2 g and the heating rate was 10 °C min^{-1}. Before performing a TPR experiment, the sample was first calcined in situ at 500 °C for 1 h under an O_2 flow of 30 ml min^{-1}, followed by cooling in the same atmosphere to room temperature. The thermal conductivity response was calibrated using the complete reduction of CuO powder (Aldrich, 99.995%).

2.3. Oxidation state titration of Co and Mn ions

The content of Mn^{4+} was determined by digesting the sample in a known excess of Mohr's salt ($Fe(NH_4)_2(SO_4)_2{\cdot}6H_2O$) standard solution acidified with 1 M H_2SO_4 and back titrating the excess of Fe^{2+} with 0.0167 M $K_2Cr_2O_7$ in 3 M HCl [19,28]. Before back titration, a small amount of H_2SO_4–H_3PO_4 mixed solution was added, 0.5% sodium diphenylamine sulfonate solution was used as indicator. The Co^{3+} concentration of the sample was determined by the iodometric titration method [28]. The experimental error of metal ion oxidation state determination was estimated to be ±0.10% for Mn and ±0.50% for Co.

2.4. Catalytic evaluation

The catalytic activity measurements were carried out at atmospheric pressure with 0.1–0.2 g (40–60 mesh) of the catalyst in a continuously flowing fixed-bed quartz microreactor (i.d. 8 mm). To minimize the effect of hot spots, an equal amount of quartz sands was mixed with the catalyst particles. The total flow rate of the reactant mixture, 1000 ppm ethylacetate (EA) + O_2 + N_2 (balance), was 33.3 ml min^{-1}, with the corresponding EA/O_2 molar ratio = 1/400 and the space velocity = 20,000 h^{-1}. The 1000 ppm EA was generated by passing a N_2 flow through a bottle containing pure EA (AR) which was placed in an ice-water isothermal bath. Reactants and product mixture were analyzed on-line by a gas chromatograph (GC-14, Shimadzu), equipped with a flame ionization detector (FID) and a thermal conductivity detector (TCD), using a (1/8) in. Chromosorb 101 column (3 m) for VOCs and a (1/8) in. Carboxen 1000 column (3 m) for permanent gas, respectively. For the variation of space velocity, we changed the mass of the catalyst at a fixed flow rate. The balance of carbon throughout the catalytic system was estimated to be 99.5%.

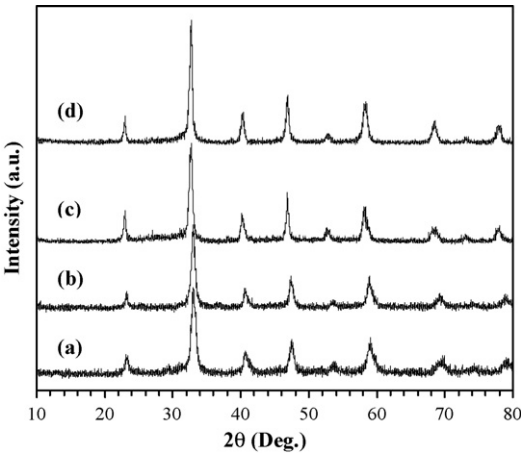

Fig. 1. XRD patterns of (a) $LaCoO_{2.91}$, (b) $La_{0.6}Sr_{0.4}CoO_{2.78}$, (c) $LaMnO_{3.12}$, and (d) $La_{0.6}Sr_{0.4}MnO_{3.02}$.

3. Results

3.1. Crystal structures, oxygen defects, surface areas, and morphologies of the catalysts

Table 1 summarizes the crystal structures, compositions, oxygen nonstoichiometry, and surface areas. By comparing the XRD patterns with the ICDD (Fig. 1) PDF Database data of $LaCoO_3$ (No. 25-1060) and $LaMnO_{3.15}$ (No. 32-484), we deduced that the $La_{1-x}Sr_xMO_{3-\delta}$ (M = Co, Mn; $x = 0$, 0.4) catalysts synthesized, in the present work, were single-phase rhombohedral perovskite-type structure. According to the principle of electroneutrality, the amount of oxygen nonstoichiometry (δ) was estimated to be 0.09 for $LaCoO_{3-\delta}$, 0.22 for $La_{0.6}Sr_{0.4}CoO_{3-\delta}$, −0.12 for $LaMnO_{3-\delta}$, and −0.02 for $La_{0.6}Sr_{0.4}MnO_{3-\delta}$. The δ values indicate that the Co-based catalysts are reductive nonstoichiometry (i.e., there are oxygen vacancies in $La_{1-x}Sr_xCoO_{3-\delta}$ [10]) whereas the Mn-based

Table 1
Physical properties of the catalysts

Catalyst	Crystal phase	Co^{3+}/Co^{2+} (mol.%/mol.%)	Mn^{4+}/Mn^{3+} (mol.%/mol.%)	δ	Surface area ($m^2\ g^{-1}$)
$LaCoO_{3-\delta}$	Rhombohedral	82.7/17.3	–	0.09	26.4
$La_{0.6}Sr_{0.4}CoO_{3-\delta}$	Rhombohedral	96.4/3.6	–	0.22	20.2
$LaMnO_{3-\delta}$	Rhombohedral	–	23.5/76.5	−0.12	32.5
$La_{0.6}Sr_{0.4}MnO_{3-\delta}$	Rhombohedral	–	41.3/59.7	−0.02	31.5

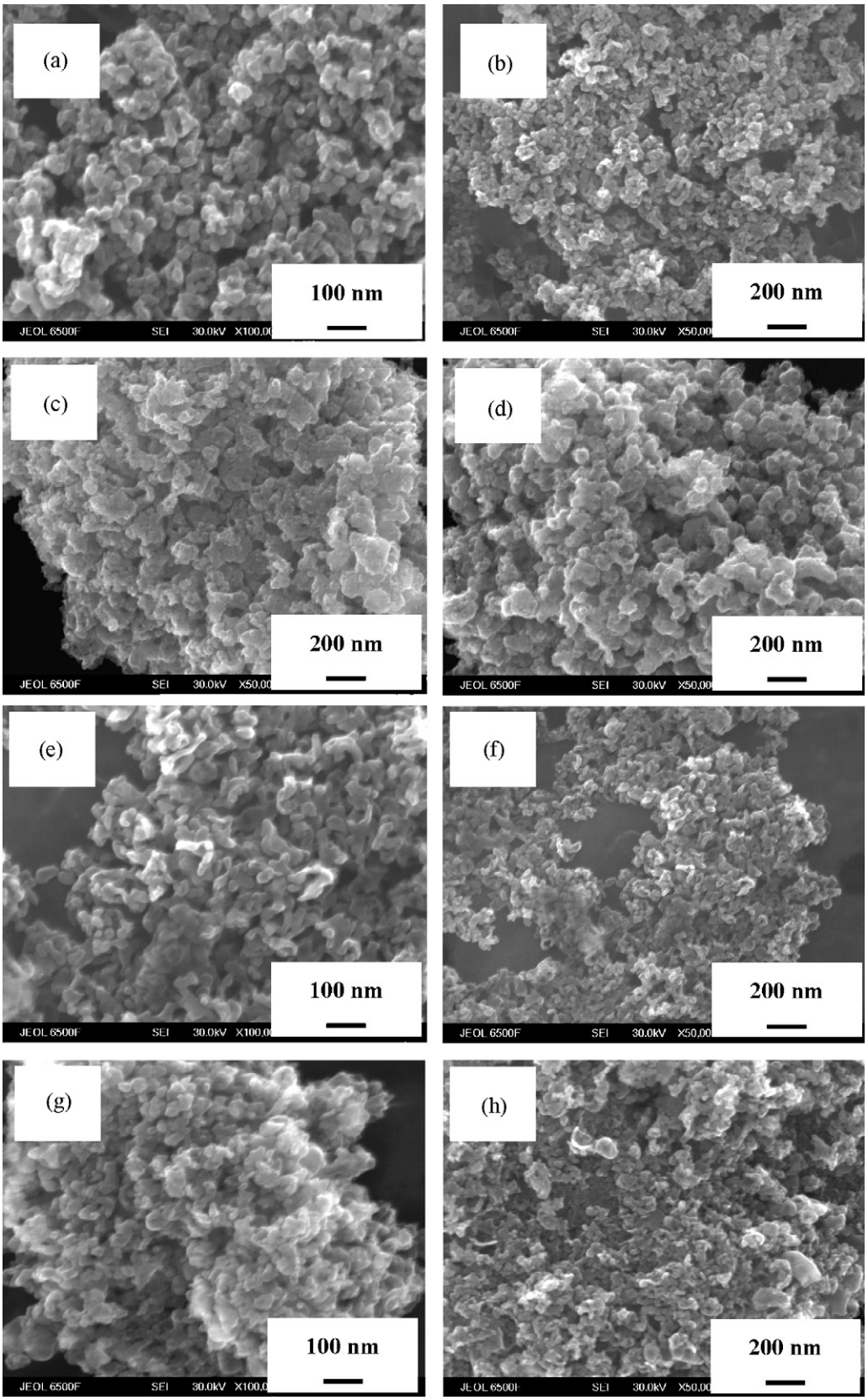

Fig. 2. HRSEM images of (a, b) $LaCoO_{2.91}$, (c, d) $La_{0.6}Sr_{0.4}CoO_{2.78}$, (e, f) $LaMnO_{3.12}$, and (g, h) $La_{0.6}Sr_{0.4}MnO_{3.02}$. The amplification magnitude was 100,000 times for images (a, c, e, g) and 50,000 times for images (b, d, f, h).

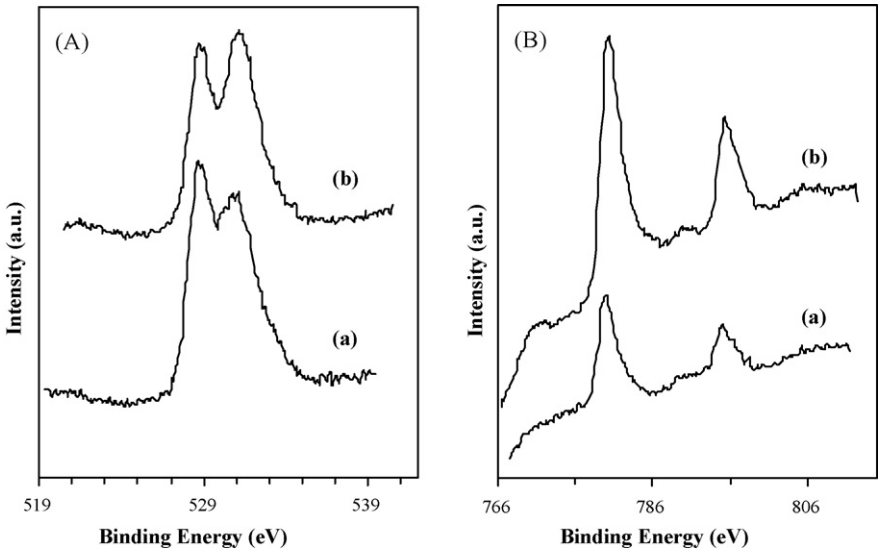

Fig. 3. (A) O 1s and (B) Co 2p XPS spectra of (a) $LaCoO_{2.91}$ and (b) $La_{0.6}Sr_{0.4}CoO_{2.78}$.

catalysts are oxidative nonstoichiometry (i.e., there are over-stoichiometric oxygen or cationic vacancies in $La_{1-x}Sr_xMnO_{3-\delta}$ [29,30]).

The surface areas of the four catalysts were rather high, ranging from 20.2 to 32.5 $m^2\ g^{-1}$. The introduction of Sr into the lattice of $LaCoO_{3-\delta}$ resulted in a significant drop in surface area, but doping Sr into the $LaMnO_{3-\delta}$ lattice induced only a very small change in surface area. Furthermore, it is observed that the Mn-based catalysts possessed much higher surface areas than the Co-based ones. Fig. 2 shows the SEM images of the $La_{1-x}Sr_xMO_{3-\delta}$ (M = Co, Mn; $x = 0$, 0.4) catalysts. It can be seen that the particles of $LaCoO_{2.91}$ (Fig. 2(a and b)) and $LaMnO_{3.12}$ (Fig. 2(e and f)) were uniform in size and short rod-shaped with a chained structure; the diameter and length were ranged 20–40 and 40–80 nm, respectively. After Sr doping, the morphology of $La_{0.6}Sr_{0.4}CoO_{2.78}$ (Fig. 2(c and d)) was changed to an irregularly lamellar shape with the typical particle sizes in the 50–100 nm range and aggregation to a certain extent took place, causing the surface area to drop greatly; most of the $La_{0.6}Sr_{0.4}MnO_{3.02}$ particles (Fig. 2(g and h)), however, remained similar morphology to $LaMnO_{3.12}$, only a few of them grew into larger lamellar particles, hence resulting in a small decrease in surface area.

3.2. Surface oxygen species, Co and Mn ion oxidation states, and reducibility of the catalysts

Fig. 3 illustrates the O 1s and Co 2p XPS spectra of the Co-based catalysts. In the C 1s spectra (not shown here), in addition to the signal (binding energy (BE) = 284.6 eV) due to adventitiously polluted carbon, there was a very weak signal at BE = 289.1 eV assignable to CO_3^{2-} with the ratio in C 1s signal intensity of the polluted carbon to that of the $CO_3^{2-} \approx 18/1$ (similar results were observed in other catalysts

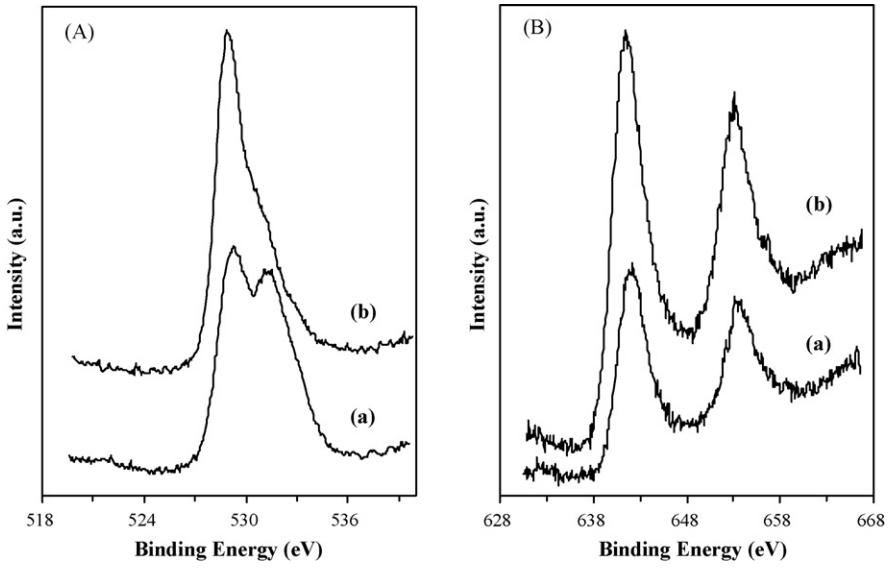

Fig. 4. (A) O 1s and (B) Mn 2p XPS spectra of (a) $LaMnO_{3.12}$ and (b) $La_{0.6}Sr_{0.4}MnO_{3.02}$.

in the present study). It indicates that the amount of residual carbonate was rather low, i.e., the contribution of carbonate to the O 1s signal would be little. As can be seen from the O 1s spectra (Fig. 3A), there were two signals at binding energy (BE) = 528.7 and 531.0 eV, corresponding to surface lattice oxygen and adsorbed oxygen species (such as O^-, O_2^-, or O_2^{2-}), respectively [31–33]; with the partial substitution of La by Sr, the intensity of the signal at higher binding energy increased whereas that at lower binding energy decreased, meaning that the amount of adsorbed oxygen species increased after Sr doping. From Fig. 3B, one can observe four signals at BE = 780.0 eV (strong, main peak), 789.6 eV (weak, satellite peak (characteristic of Co^{2+})), 795.0 eV (strong, main peak), and 805.0 eV (very weak, satellite peak (characteristic of Co^{2+})), the former two belong to Co $2p_{3/2}$ whereas the latter two are due to Co $2p_{1/2}$ [34]. The asymmetric main peaks at BE = 780.0 and 795.0 eV imply the presence of multi-components that could be resolved into two components, assignable to the signals due to Co^{3+} and Co^{2+} ions, respectively [34]. Therefore, there were Co^{3+} and Co^{2+} ions present in the Co-based catalysts. One can also observe that with the inclusion of Sr in the perovskite lattice, the signal intensities of Co $2p_{3/2}$ and Co $2p_{1/2}$ increased significantly (Fig. 3B(b)), indicating the rise in Co^{3+} concentration. This is in agreement with the chemical analysis results of cobalt ion distributions (Table 1).

Shown in Fig. 4 are the O 1s and Mn 2p XPS spectra of the Mn-based catalysts. It is seen that there were two signal peaks at 528.9 and 531.0 eV (Fig. 4A(a)), which could be assigned to surface lattice oxygen and adsorbed oxygen species, respectively [31–33]; after Sr doping, the intensity of the signal at BE = 531.0 eV decreased (Fig. 4A(b)), indicating a drop in the amount of adsorbed oxygen species. From Fig. 4B, one can observe the appearance of two signals at BE = 641.3 and 653.3 eV, assignable to Mn $2p_{3/2}$ and Mn $2p_{1/2}$, respectively [35,36]; the asymmetry of the two peaks indicates the existence of mixed components: the former could be resolved into two components at BE = 641.1 and 642.6 eV, whereas the latter into the ones at BE = 653.0 and 654.4 eV. The signals at BE = 641.1 and 653.0 eV were attributable to Mn^{3+} ions, whereas the ones at BE = 642.6 and 654.4 eV to Mn^{4+} ions [35,36]. Similar to the case in the Co-based catalysts, Sr doping into the $LaMnO_{3-\delta}$ lattice resulted in a rise in signal intensity (Fig. 4B(b)), i.e., an increase in Mn^{4+} concentration.

Fig. 5 illustrates the O_2-TPD profiles of the $La_{1-x}Sr_xMO_{3-\delta}$ catalysts. There was a weak broad desorption peak at 190 °C and a desorption peak at 873 °C over $LaCoO_{2.91}$ (Fig. 5a), with the O_2 desorption of 5.9 and 11.9 μmol g_{cat}^{-1}, respectively; after Sr doping, there were three desorption peaks at 182, 556, and 838 °C (Fig. 5b), the corresponding O_2 desorption amount was 67.3, 100.9, and 268.8 μmol g_{cat}^{-1}; over $LaMnO_{3.12}$, a small peak at 205 °C and a big peak at 418 °C were recorded, with a total amount of O_2 desorption = 262.3 μmol g_{cat}^{-1}, furthermore a big desorption started from 630 °C (Fig. 5c); over $La_{0.6}Sr_{0.4}MnO_{3.02}$, there were two desorption peaks at 219 and 600 °C (Fig. 5d) with the latter much broader than the former, the O_2 desorption amount was 22.0 and 415.8 μmol g_{cat}^{-1}, respectively. The peaks below 400 °C could be attributed to the

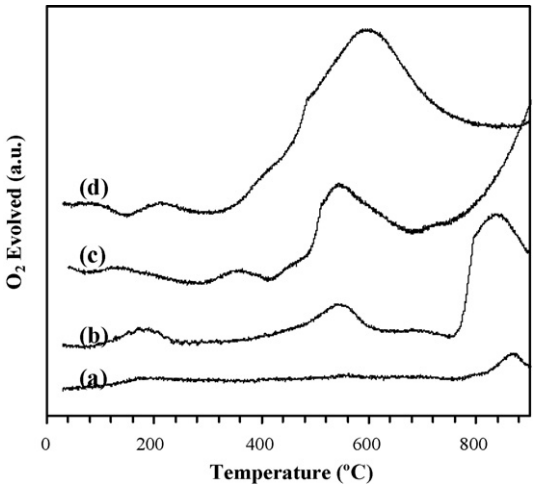

Fig. 5. O_2-TPD profiles of (a) $LaCoO_{2.91}$, (b) $La_{0.6}Sr_{0.4}CoO_{2.78}$, (c) $LaMnO_{3.12}$, and (d) $La_{0.6}Sr_{0.4}MnO_{3.02}$.

desorption of oxygen species adsorbed at surface vacancies, the ones in the range of 400–750 °C to the desorption of surface lattice oxygen due to partial reduction of Co^{3+} or Mn^{4+}, above 750 °C they were the desorption of lattice oxygen due to the reduction of Co^{2+} or Mn^{4+} left [37].

Fig. 6 shows the TPR profiles of the $La_{1-x}Sr_xMO_{3-\delta}$ catalysts. It is observed that there were big reduction bands at 434 and 645 °C (with a shoulder at 711 °C) over $LaCoO_{2.91}$ (Fig. 6a), the corresponding amount of H_2 consumed was 1.80 and 3.57 mmol g_{cat}^{-1}; over $La_{0.6}Sr_{0.4}CoO_{2.78}$, there appeared a very weak reduction band at 172 °C, a big reduction band at 371 °C, two sharp reduction bands at 522 and 594 °C, a shoulder at 680 °C and a weak reduction band at 855 °C (Fig. 6b), the total amount of H_2 consumption was 2.22 mmol g_{cat}^{-1} for the former two bands and 4.87 mmol g_{cat}^{-1} for the latter four bands; over $LaMnO_{3.12}$, two reduction bands were recorded at 450 and 887 °C (Fig. 6c), corresponding to the H_2 consumption of 1.57 and 1.21 mmol g_{cat}^{-1}; as can be seen in Fig. 6d, the doping of Sr into the $LaMnO_{3-\delta}$ lattice gave rise to five reduction bands at 180 °C (very weak), 297 °C (strong),

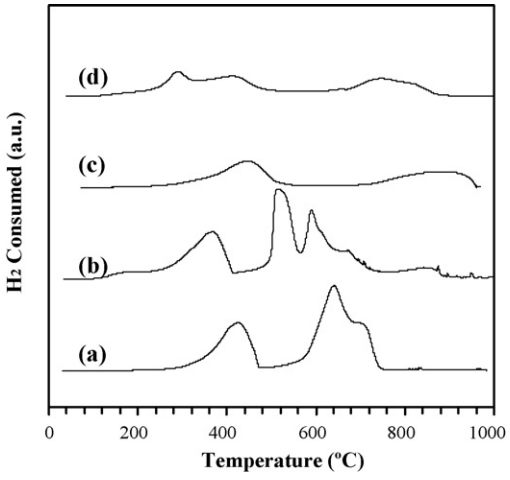

Fig. 6. TPR profiles of (a) $LaCoO_{2.91}$, (b) $La_{0.6}Sr_{0.4}CoO_{2.78}$, (c) $LaMnO_{3.12}$, and (d) $La_{0.6}Sr_{0.4}MnO_{3.02}$.

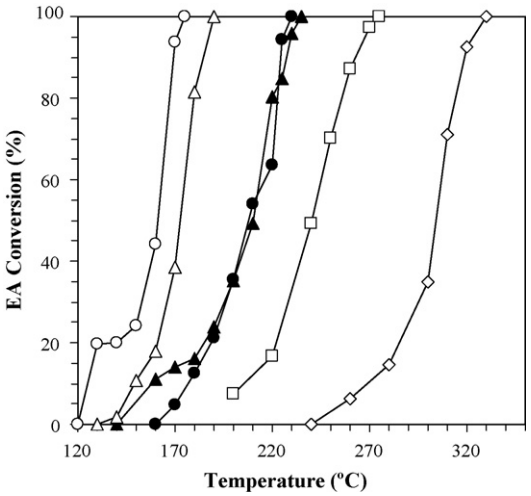

Fig. 7. Catalytic performance of $LaCoO_{2.91}$ (●), $La_{0.6}Sr_{0.4}CoO_{2.78}$ (○), $LaMnO_{3.12}$ (▲), and $La_{0.6}Sr_{0.4}MnO_{3.02}$ (△) as well as $La_{0.6}Sr_{0.4}CoO_{3-\delta}$ (◇) and $La_{0.6}Sr_{0.4}MnO_{3-\delta}$ (□) that were calcined at 900 °C for 4 h as a function of reaction temperature at EA concentration = 1000 ppm, EA/O_2 molar ratio = 1/400, and space velocity = 20,000 h^{-1}.

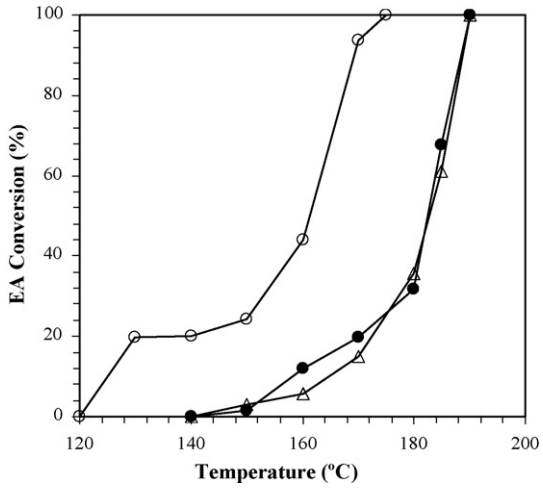

Fig. 8. Catalytic performance of $La_{0.6}Sr_{0.4}CoO_{2.78}$ as a function of reaction temperature at various space velocities (20,000 h^{-1} (○), 40,000 h^{-1} (●), and 80,000 h^{-1} (△)) under the conditions of EA concentration = 1000 ppm and EA/O_2 molar ratio = 1/400.

422 °C (strong), 757 °C (strong), and 823 °C (shoulder), the former three correspond to the H_2 consumption of 2.06 mmol g_{cat}^{-1} whereas the latter two to that of 1.28 mmol g_{cat}^{-1}. . The bands below 500 °C were due to the reduction of oxygen adspecies and the partial reduction of Mn^{4+} to Mn^{3+} or Co^{3+} to Co^{2+} whereas the ones above 500 °C to the reduction of the Mn^{4+} left or Co^{2+} [24].

3.3. Catalytic performance for the EA oxidation

Fig. 7 shows the catalytic activities of $La_{1-x}Sr_xMO_{3-\delta}$ for the oxidation of EA. Under the reaction conditions of EA concentration = 1000 ppm, EA/O_2 molar ratio = 1/400, and space velocity = 20,000 h^{-1}, the EA conversion increased with the rise in temperature, the Sr-doped Co-based catalyst performed the best. The catalytic performance followed a sequence of $La_{0.6}Sr_{0.4}CoO_{2.78} > La_{0.6}Sr_{0.4}MnO_{3.02} > LaCoO_{2.91} \approx LaMnO_{3.12}$. The light-off temperature $T_{50\%}$ (EA conversion = 50%) and complete removal temperature $T_{100\%}$ (EA conversion = 100%) were 162 and 175 °C over $La_{0.6}Sr_{0.4}CoO_{2.78}$, 173 and 190 °C over $La_{0.6}Sr_{0.4}MnO_{3.02}$, 209 and 230 °C over $LaCoO_{2.91}$, and 210 and 235 °C over $LaMnO_{3.12}$, respectively. For the sake of comparison, we also examined the catalytic activities of the Sr-doped cobaltite (surface area = 7.2 $m^2\ g^{-1}$) and manganite (surface area = 9.8 $m^2\ g^{-1}$) catalysts that had been calcined at 900 °C for 4 h (hence they were large-size particles, although no further characterization was made). Apparently, these materials performed much interior to their counterparts calcined at 650 °C for 2 h and the Co-based catalyst was much more active than the Mn-based one. It is worthy to point out that in addition to CO_2 and H_2O, no partially oxidized products were detected over our nanoperovskite catalysts in the oxidation of EA, as confirmed by the estimated carbon balance of 99.5%.

Shown in Fig. 8 is the effect of space velocity on the activity of the best-performing catalyst $La_{0.6}Sr_{0.4}CoO_{2.78}$. At each of the three space velocities examined, the EA conversion augmented with increasing reaction temperature. The catalytic activity decreased with the rise in space velocity, but no significant decrease in activity was observed if space velocity further increased from 40,000 to 80,000 h^{-1} where the $T_{50\%}$ and $T_{100\%}$ were 183 and 190 °C, respectively.

4. Discussion

Among the A-site-substituted $LaMO_{3-\delta}$ (M = Co, Mn) series, Sr-substitution for La has been studied most extensively and intensively [37]. The partial substitution of Sr^{2+} for La^{3+} is expected to increase the oxygen vacancy density of $LaCoO_{3-\delta}$ ($\delta > 0$) and to reduce the excess nonstoichiometric oxygen amount of $LaMnO_{3-\delta}$ ($\delta < 0$), as substantiated by the data in Table 1. The Sr-substitution increased the Co^{3+} and Mn^{4+} contents, resulting in a rise in the amount of oxygen nonstoichiometry in $La_{0.6}Sr_{0.4}CoO_{3-\delta}$ and a drop in the amount of over-stoichiometric oxygen (i.e., cationic vacancies) in $La_{0.6}Sr_{0.4}MnO_{3-\delta}$. All the catalysts investigated, in the present work, possessed rhombohedral crystal structure, same as those reported by Spinicci et al. [19]. With fairly good crystallinity, the surface areas of $La_{1-x}Sr_xMO_{3-\delta}$ were still rather high (20–33 $m^2\ g^{-1}$), demonstrating that the citric acid complexing-hydrothermal-coupled strategy is suitable for the generation of high-surface-area perovskite-type oxide nanoparticles, because by adopting either the citric acid complexing method or the hydrothermal method we could not obtain such high surface areas with similar crystallinity (e.g., citric acid complexing method: 11.0 $m^2\ g^{-1}$; hydrothermal method: 12.3 $m^2\ g^{-1}$ for $LaMnO_{3-\delta}$ after 700 °C calcination). We speculate that the complexing action of citric acid with metal ions would facilitate the formation of uniform co-precipitation of metal ions when ammonia was added. The obvious decrease in surface area after Sr-doping to the $LaCoO_{3-\delta}$ lattice might be associated with the difference in the complexing ability of La,

Sr, and Co ions with citric acid. A direct observation for the high surface areas of the $La_{1-x}Sr_xMO_{3-\delta}$ catalysts is from the SEM images (Fig. 2). $LaCoO_{2.91}$ and $LaMnO_{3.12}$ were uniform nanoparticles. After Sr doping, there were changes in morphology and size of the cobaltite particles (causing the surface area to drop), but no significant changes were detected in morphology and size of the manganite particles (bringing about only a small drop in surface area).

The Co $2p_{3/2}$ (or Co $2p_{1/2}$) transition is characterized by a main peak with a satellite at higher BE for cobalt in bivalent chemical state [38,39]. The main and satellite peaks can be related, respectively, to $2p^53d^8\underline{L}$ ($\underline{L}$ means a ligand hole) and $2p^53d^7$ electronic configurations in the final state [40]. The appearance of the satellite peak is an indication of Co^{2+} presence. From the XPS spectra of Co 2p in the Co-based catalysts (Fig. 3B), one can observe that the Co $2p_{3/2}$ (or Co $2p_{1/2}$) main peaks were asymmetrical and the satellite intensities were rather low. The sharp and more intense component at lower BE is ascribed to Co^{3+}, whereas the shoulder at higher BE represents the Co^{2+} component [34]. With the doping of strontium, the signal of Co^{3+} intensified, meaning that the amount of Co^{3+} ions increased, in agreement with the results of cobalt oxidation state titration (Table 1). Similarly, in the case of $La_{1-x}Sr_xMnO_{3-\delta}$, Sr-doping enhanced the content of Mn^{4+} ions (Table 1), in agreement with the phenomena that Mn^{4+} signal intensity increased after Sr-doping (Fig. 4B). Due to that the BEs of O^-, O_2^-, and O_2^{2-} species are rather close, one cannot differentiate them just only based on the BE values. Most researchers believe that the oxygen species at oxygen vacancies of ABO_3 are dissociatively adsorbed oxygen [10,41], i.e., O^-. Since the catalysts had been thermally treated in an O_2 flow at high temperature and during the recording of XPS spectra, these samples were not exposed to the air, one can leave out the presence of OH^- on catalyst surfaces. Furthermore, there was little amount of carbonate in the catalysts. Therefore, we may think that the oxygen species over the Co-based catalysts were mainly O^-. From the O 1s XPS spectra, one can realize that the doping of Sr increased the amount of surface adsorbed oxygen species over the cobaltite catalyst (Fig. 3A), whereas it decreased over the Sr-doped manganite catalyst where the cationic defect density decreased (Fig. 4A). In other words, the amount of surface oxygen adspecies follows the order of $La_{0.6}Sr_{0.4}CoO_{2.78} > LaCoO_{2.91}$ and $LaMnO_{3.12} > La_{0.6}Sr_{0.4}MnO_{3.02}$, coinciding with the results obtained in the O_2-TPD investigation.

It is generally believed that the oxidation of organic compounds proceeds via the interaction of adsorbed organic compounds with adsorbed and lattice oxygen [42–48]. The former is oxygen adsorbed dissociatively at oxygen vacancies, usually called α oxygen in O_2-TPD studies [32,49–51]. This kind of oxygen species is generally thought to be responsible for the total oxidation of hydrocarbons and oxygenates. The latter is generally called β oxygen in O_2-TPD studies and can be related to the partial reduction of B-site cation [50,51]. It has been reported that the redox reactions of cobalt or manganese ions with lattice oxygen in $La_{1-x}A'_xMO_{3-\delta}$ ($A' = Ca, Sr$; $M = Mn, Fe, Co$) play an important role in enhancing ammoxidation activity [28]. We suggest that the catalytic activities of $La_{1-x}Sr_xMO_{3-\delta}$ could be attributed to the extent of the redox processes: $Co^{3+} \Leftrightarrow Co^{2+}$ and $Mn^{4+} \Leftrightarrow Mn^{3+}$. That is to say, the redox properties of Co and Mn ions (related to the Co^{3+}/Co^{2+} and Mn^{4+}/Mn^{3+} ratios in the catalysts) exert significant influence on the catalytic performance. Working on the reactivity of lattice oxygen and the desorption of oxygen over cobaltite perovskites, Nakamura et al. [52] concluded that lattice oxygen involvement, cobalt ion reduction, and oxygen vacancy formation took place concurrently in the oxidation process of CO. With the generation of surface vacancies, the diffusion of lattice oxygen from the bulk to the surface would become facile and the surface oxygen consumed in the reaction could be replenished readily. As illustrated in the O_2-TPD studies (Fig. 5(a and b)), the extent of α oxygen desorption over $La_{0.6}Sr_{0.4}CoO_{2.78}$ (67.3 μmol g_{cat}^{-1}) was much larger than that over $LaCoO_{2.91}$ (5.9 μmol g_{cat}^{-1}), indicating that the amount of oxygen vacancies in the former was higher than that in the latter. The desorption of lattice oxygen induced the partial reduction of Co^{3+} to Co^{2+} or Mn^{4+} to Mn^{3+}. The amount of β oxygen desorption over $La_{0.6}Sr_{0.4}CoO_{2.78}$ (367.7 μmol g_{cat}^{-1}) was much larger than that over $LaCoO_{2.91}$ (11.9 μmol g_{cat}^{-1}), indicating that the incorporation of Sr^{2+} into the $LaCoO_{3-\delta}$ lattice promoted the activity (mobility) of lattice oxygen. Furthermore, the reduction temperature of $La_{0.6}Sr_{0.4}CoO_{2.78}$ (Fig. 6b) was much lower than that of $LaCoO_{2.91}$ (Fig. 6a), confirming that the activity of lattice oxygen in the former catalyst was higher than that in the latter catalyst. The feasibility of bulk reduction (by H_2) at ca. 370 °C (Fig. 6b) is indicative of high activity of the lattice oxygen in $La_{0.6}Sr_{0.4}CoO_{2.78}$. Similar scenario is present in the case of $La_{1-x}Sr_xMO_{3-\delta}$ (Figs. 5(c and d) and 6(c and d)). Another piece of supporting evidence is from one of our previous work related to the $^{18}O/^{16}O$ isotopic exchange and $^{18}O_2$/CO pulsing over $La_{0.6}Sr_{0.4}Co_{0.8}Bi_{0.2}O_{2.80}$: the facile infiltration of ^{18}O into the perovskite lattice and the rapid replenishment of the consumed amount of lattice oxygen by gas-phase oxygen demonstrate the high activity of lattice oxygen in the perovskite-type oxide catalyst [24].

Compared to the activation of organic compounds, O_2 could be activated readily at structural defects of perovskite catalysts. Since the decrease in surface oxygen concentration undermines the process of lattice oxygen replenishment, therefore, it is understandable that in an O_2-rich atmosphere, VOC oxidation could proceed at a relative lower temperature [19]. In the products of EA oxidation over our catalysts, only CO_2 and H_2O were detected, no any partially oxidized products were generated. As shown in Fig. 7, $La_{0.6}Sr_{0.4}CoO_{3-\delta}$ and $La_{0.6}Sr_{0.4}MnO_{3-\delta}$ (large-size particles) calcined at 900 °C for 4 h exhibited catalytic performance much lower than $La_{0.6}Sr_{0.4}CoO_{2.78}$ and $La_{0.6}Sr_{0.4}MnO_{3.12}$ (nanoparticles). It might be due to the fact that compared to the conventional large-size ABO_3 particles, the nanometer $La_{1-x}Sr_xMO_{3-\delta}$ catalysts possess more surface coordination-unsaturated atoms and hence render the EA molecules as well as oxygen molecules more easily activated, resulting in the total oxidation of EA at lower temperatures. Under the reaction conditions

adopted in this study, the catalytic performance follows the sequence of $La_{0.6}Sr_{0.4}CoO_{2.78}$ ($T_{100\%}$ = 175 °C) > $La_{0.6}Sr_{0.4}MnO_{3.12}$ ($T_{100\%}$ = 190 °C) > $LaCoO_{2.91}$ ($T_{100\%}$ = 230 °C) ≈ $LaMnO_{3.02}$ ($T_{100\%}$ = 235 °C) (Fig. 7). Unlike those observed over precious metal catalysts, the catalytic activities of perovskites for VOC oxidation are more sensitive to the change in space velocity. In an O_2-rich atmosphere, the $T_{100\%}$ rose with the increase in space velocity (Fig. 8). Apparently, the $La_{0.6}Sr_{0.4}CoO_{2.78}$ catalyst showed good performance for EA oxidation under oxidizing conditions. Therefore, it is suggested that the enhanced catalytic activity of $La_{0.6}Sr_{0.4}MO_{3-\delta}$ is associated with the promotion in lattice oxygen activity.

Although there are many factors to influence the catalytic performance of ABO_3, the surface area, anionic/cationic defect density, and lattice oxygen activity (related to B-site ion redox ability) are the key factors. When the ABO_3 catalysts have similar defect density and redox ability, the catalytic activity is proportional to the surface area [21]. With the changes in defect amount and redox properties, however, one cannot compare the catalytic performance only based on surface areas. As discussed above, large-surface-area $La_{1-x}Sr_xMO_{3-\delta}$ nanoparticles catalyzed the EA completely to CO_2 and H_2O, different from large-size perovskite oxide catalysts over which partially oxidized products are generated. Taking into account these considerations, we conclude that the enhancements in oxygen deficient concentration and M ion redox ability, as well as surface area render the $La_{0.6}Sr_{0.4}MO_{3-\delta}$ (M = Co, Mn) materials catalytically highly active for EA oxidation.

5. Conclusions

Nanometer perovskite-type oxides $La_{1-x}Sr_xMO_{3-\delta}$ (M = Co, Mn; x = 0, 0.4) were successfully prepared by coupling the methods of citric acid complexing and hydrothermal synthesis. All the catalysts adopted a single-phase rhombohedral perovskite structure. The $La_{1-x}Sr_xCoO_{3-\delta}$ samples possessed oxygen deficiency, whereas the $La_{1-x}Sr_xMnO_{3-\delta}$ ones showed oxygen over-stoichiometry; the doping of Sr induced an increase in oxygen vacancy density for the Co-based catalyst but caused a decrease in the amount of over-stoichiometric oxygen for the Mn-based catalyst. The surface areas (20–26 $m^2\,g^{-1}$) of $La_{1-x}Sr_xCoO_{3-\delta}$ were lower than those (32–33 $m^2\,g^{-1}$) of $La_{1-x}Sr_xMnO_{3-\delta}$, such high surface areas are due to the fact that the citric acid complexing-hydrothermally derived $La_{1-x}Sr_xMO_{3-\delta}$ catalysts were uniform with the typical particle size of 40–80 nm, as can be clearly seen in their HRSEM photographs. There were Co^{3+} and Co^{2+} ions in $La_{1-x}Sr_xCoO_{3-\delta}$ and Mn^{4+} and Mn^{3+} ions in $La_{1-x}Sr_xMnO_{3-\delta}$; Sr-substitution induced the rises in Mn^{4+} and Co^{3+} concentrations. Adsorbed oxygen species (O^-, O_2^-, or O_2^{2-}) were present on/in the catalysts. Doping Sr^{2+} into the $LaMO_{3-\delta}$ lattices resulted in the improvement of redox ability and the enhancements of adsorbed and lattice oxygen desorption at low temperatures. Under the conditions of EA concentration = 1000 ppm, EA/O_2 molar ratio = 1/400, and space velocity = 20,000 h^{-1}, the catalytic activity increased in the order of $LaCoO_{2.91}$ ($T_{100\%}$ = 230 °C) ≈ $LaMnO_{3.02}$ ($T_{100\%}$ = 235 °C) < $La_{0.6}Sr_{0.4}MnO_{3.12}$ ($T_{100\%}$ = 190 °C) < $La_{0.6}Sr_{0.4}CoO_{2.78}$ ($T_{100\%}$ = 175 °C); furthermore, there was no formation of partially oxidized by-products over these nanosized perovskite-type oxide catalysts. Based on the above results, it is concluded that in addition to the contribution of high surface areas, the excellent catalytic performance is associated with the rich structural defects and M^{n+} (M = Co, Mn) good redox ability of the $La_{1-x}Sr_xMO_{3-\delta}$ nanomaterials.

Acknowledgements

The work described above was fully supported by a grant from the Key Project of Science & Technology Development Plan of the Education Committee of Beijing Municipality and the Key Project (Class B) of Natural Science Foundation of Beijing Municipality (Grant no. KZ200610005004).

References

[1] M.J. Molina, Pure Appl. Chem. 68 (1996) 1749.
[2] R. Atkinson, Atms. Environ. 34 (2000) 2063.
[3] R.J. Farrauto, C.H. Bartholomew, Fundamentals of Industrial Catalytic Processes, Blackie Academic, London, 1997, p. 640.
[4] A.F. Dolidovich, G.S. Akhremkova, V.S. Efremtsev, Can. J. Chem. Eng. 77 (1999) 342.
[5] B.K. Hondnett, Heterogeneous Catalytic Oxidation, Fundamentals and Technological Aspects of the Selective and Total Oxidation of Organic Compounds, Wiley, Chichester, 2000, p. 191.
[6] G. Centi, P. Ciambelli, S. Perathoner, P. Russo, Catal. Today 75 (2002) 3.
[7] T. Nitadori, T. Ichiki, M. Misono, Bull. Chem. Soc. Jpn. 61 (1988) 621.
[8] N. Yamazoe, Y. Teraoka, Catal. Today 8 (1990) 175.
[9] V. Szabo, M. Bassir, A. Van Neste, S. Kaliaguine, Appl. Catal. B 37 (2002) 175.
[10] T. Seiyama, Catal. Rev. Sci. Eng. 34 (1992) 281.
[11] J.-J. Liang, H.-S. Weng, Ind. Eng. Chem. Res. 32 (1993) 2563.
[12] S. Irusta, M.P. Pina, M. Menéndez, J. Santamaría, J. Catal. 179 (1998) 400.
[13] L. Marchetti, L. Forni, Appl. Catal. B 15 (1998) 179.
[14] R. Burch, P.J.F. Harris, C. Pipe, Appl. Catal. A 120 (2001) 63.
[15] Z.L. Yu, L.Z. Gao, S. Yuan, Y. Wu, J. Chem. Soc., Faraday Trans. 88 (1992) 3245.
[16] M. O'Connell, A.K. Norman, C.F. Hutterman, M.A. Morris, Catal. Today 47 (1999) 123.
[17] P. Papaefhimiou, T. Ioannides, X.E. Verykios, Appl. Catal. B 13 (1997) 175.
[18] P. Papaefhimiou, T. Ioannides, X.E. Verykios, Appl. Catal. B 15 (1998) 75.
[19] R. Spinicci, M. Faticanti, P. Marini, S. De Rossi, P. Porta, J. Mol. Catal. A 197 (2003) 147.
[20] V. Blasin-Aubé, J. Belkouch, L. Monceaux, Appl. Catal. B 43 (2003) 175.
[21] K.R. Barnard, K. Foger, T.W. Turney, R.D. Williams, J. Catal. 125 (1990) 265.
[22] H.X. Dai, H. He, W. Li, Z.Z. Gao, C.T. Au, Catal. Lett. 73 (2001) 149.
[23] H. He, H.X. Dai, Y.L. Leung, C.T. Au, Appl. Catal. B 33 (2001) 65.
[24] H.X. Dai, H. He, P.H. Li, L.Z. Gao, C.T. Au, Catal. Today 90 (2004) 231.
[25] (a) H.X. Dai, C.F. Ng, C.T. Au, J. Catal. 189 (2000) 52;
(b) H.X. Dai, C.F. Ng, C.T. Au, J. Catal. 193 (2000) 65;
(c) H.X. Dai, C.F. Ng, C.T. Au, J. Catal. 197 (2001) 251.
[26] (a) H.X. Dai, C.F. Ng, C.T. Au, Catal. Lett. 57 (1999) 115;
(b) H.X. Dai, C.F. Ng, C.T. Au, Catal. Lett. 67 (2000) 183.
[27] H.X. Dai, C.T. Au, Y. Chan, K.C. Hui, Y.L. Leung, Appl. Catal. A 213 (2001) 91.
[28] Y. Wu, T. Yu, B.S. Dou, C.X. Wang, X.F. Xie, Z.L. Yu, S.R. Fan, Z.R. Fan, L.C. Wang, J. Catal. 120 (1989) 120.
[29] B.C. Tofield, W.R. Scott, J. Solid State Chem. 10 (1974) 183.

[30] J.A.M. van Roosmalen, E.H.P. Cordfunke, R.B. Helmoldt, H.W. Zandbergen, J. Solid State Chem. 110 (1994) 100.
[31] A.F. Carley, M.W. Roberts, A.K. Santra, J. Phys. Chem. B 101 (1997) 9978.
[32] N. Yamazoe, Y. Teraoka, T. Seiyama, Chem. Lett. (1981) 1767.
[33] J.L.G. Fierro, L.G. Tejuca, Appl. Surf. Sci. 27 (1987) 453.
[34] G. Fierro, M. Lo Jacono, M. Inversi, R. Dragone, P. Porta, Top. Catal. 10 (2000) 39.
[35] J.F. Moulder, W.F. Stickle, P.E. Sobol, K.D. Bomben, in: J. Chastain, R.C. King, Jr. (Eds.), Handbook of X-ray Photoelectron Spectroscopy, Physical Electronics, Inc., Eden Prairie, 1995.
[36] J.C. Carver, G.K. Schweitzer, J. Chem. Phys. 57 (1972) 973.
[37] L.G. Tejuca, J.L.G. Fierro (Eds.), Properties and Applications of Perovskite-Type Oxides, Dekker, New York, 1993.
[38] A. Cimino, B.A. De Angelis, G. Minelli, Surf. Interf. Anal. 5 (1983) 150.
[39] D.C. Frost, A. Ishitani, C.A. McDowell, Mol. Phys. 24 (1972) 861.
[40] G. Fierro, R. Dragone, G. Moretti, P. Porta, Surf. Interf. Anal. 19 (1992) 565.
[41] H.M. Zhang, Y. Shimizu, Y. Teraoka, N. Miura, N. Yamazoe, J. Catal. 121 (1990) 432.
[42] Y.J. Mergler, A. van Aalst, J. van Delft, B.E. Nieuwenhuys, Appl. Catal. B 10 (1996) 245.
[43] Y.J. Mergler, J. Hoebink, B.E. Nieuwenhuys, J. Catal. 167 (1997) 305.
[44] T. Jin, T. Okuhara, G.J. Mains, J.M. White, J. Phys. Chem. 91 (1987) 3310.
[45] S.H. Oh, C.C. Eickel, J. Catal. 112 (1988) 543.
[46] G.S. Zafiris, R.J. Gorte, J. Catal. 143 (1993) 86.
[47] C. Serre, F. Garin, G. Belot, G. Maire, J. Catal. 141 (1993) 9.
[48] A.K. Tripathi, N.M. Gupta, J. Catal. 153 (1995) 208.
[49] C.N.R. Rao (Ed.), Chemistry of Oxide Superconductivity, Blackwell, Oxford, 1988.
[50] A. Bielañski, J. Haber, Oxygen in Catalysis, Dekker, New York, 1991.
[51] J. Haber, in: J.P. Bonnelle, B. Delmon, E. Derouane (Eds.), Surface Properties and Catalysis by Non-Metals, Reidel, Dordrecht, 1983.
[52] T. Nakamura, M. Misono, Y. Yoneda, Chem. Lett. (1981) 1589.